Journal of Marine Research, 48, 765–791, 1990

Deep Western Boundary Current variability at Cape Hatteras

by Robert S. Pickart[1,2] and D. Randolph Watts[2]

ABSTRACT

Data from an array of inverted echo sounders and bottom current meters off Cape Hatteras, where the Gulf Stream and Deep Western Boundary Current (DWBC) cross each other, are analyzed to investigate the deep components of flow. While the mean flow is to the southwest with the DWBC, the observed temporal variability is dominated by energetic 40 day topographic Rossby waves. By optimally weighting the individual deep current meter measurements, the deep flow is averaged across the wavelength of the 40 day wave, thereby reducing the wave signal and revealing variations of the spatially averaged DWBC. The DWBC fluctuations are found to be oriented more along the isobaths than the wave motions (which have an essential cross-isobath component). Lateral path displacements of the upper layer Gulf Stream, as measured by the inverted echo sounders, are correlated with deep velocity and temperature fluctuations at specific sites, which can be understood in terms of deep Gulf Stream influence. Cross-slope flow of the spatially averaged DWBC is found to vary with changes in angle of the Gulf Stream path in a manner consistent with simple dynamics.

1. Introduction

The existence of mean abyssal currents along the western boundaries of the world ocean, originally postulated by Stommel (1958) to balance interior upwelling, has now been well documented observationally. The North Atlantic Deep Western Boundary Current (DWBC), in particular, has been studied using a variety of measurement techniques. The deepest component of the DWBC is comprised of a mixture of Denmark Straits and Iceland-Scotland overflow water (Worthington, 1970; Swift, 1986) which flows around the Grand Banks of Newfoundland and under the Gulf Stream at Cape Hatteras. West of the Grand Banks—several thousand kilometers from its source region—the current is substantially diluted from past entrainment and mixing, however it is still identifiable by an anomalous property and velocity core (e.g. Pickart *et al.*, 1989; Roemmich and Wunsch, 1985). In this region the DWBC core is found at a depth of 3000–3500 m, with a potential temperature of ~2.0–2.5°C.

The DWBC was first observed directly using neutrally buoyant floats (Swallow and

1. Present address: Woods Hole Oceanographic Institution, Woods Hole, Massachusetts, 02543, U.S.A.
2. Graduate School of Oceanography, University of Rhode Island, Narragansett, Rhode Island, 02882, U.S.A.

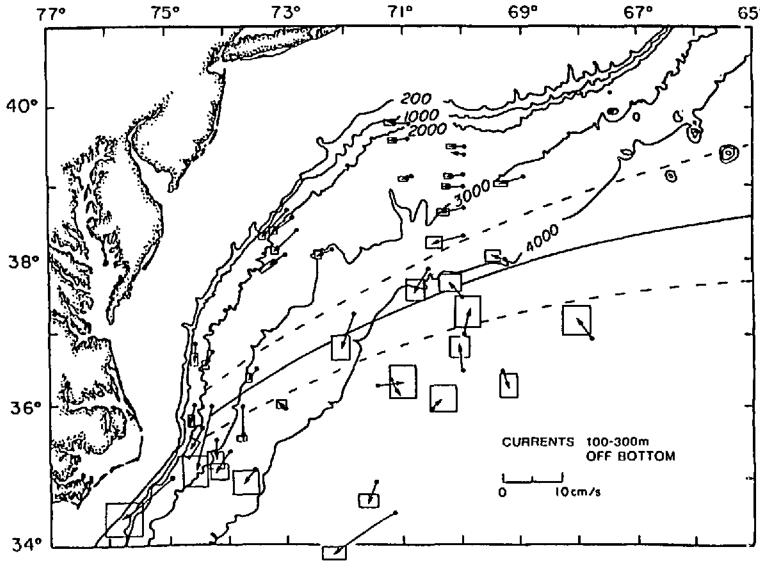

Figure 1. Mean current meter velocities 100–300 m off the bottom from historical measurements collected in the middle Atlantic Bight (from Watts, 1989). The record lengths of the measurements vary from 4 months to 2 years, and the box associated with each vector represents the uncertainty of the mean, typically 1–2 cm/sec. The number of degrees of freedom used to compute the error bars was estimated from the integral time scales.

Worthington, 1961; Barrett, 1965); evidence of the increased flow at depth has also been identified geostrophically at numerous locations (e.g. Worthington, 1976; Roemmich and Wunsch, 1985). Because the water comprising the DWBC has been in recent contact with the atmosphere it is characterized by a high oxygen content as well as high concentrations of chlorofluorocarbons and tritium. Thus, property sections taken across the continental boundary nicely reveal this anomalous water mass adjacent to the slope.

Many direct current meter measurements within the DWBC in the western North Atlantic have also now been made. It is evident that there is mean equatorward flow along the entire continental slope. Figure 1 shows a compilation of historical mean deep current meter measurements from the Mid-Atlantic Bight (from Watts, 1989); shoreward of the 4000 m isobath the flow is everywhere equatorward (with one exception of insignificant flow upslope). It is interesting to note, however, that in general the mean DWBC speeds measured by current meters (e.g. 5–10 cm/sec; Luyten, 1977) are substantially weaker than typical synoptic velocity estimates (e.g. 20 cm/sec; Joyce *et. al.*, 1986). This may be due in part to variability of the DWBC itself, but it is now well known that energetic topographic Rossby waves (TRWs) are also present along the continental slope west of the Grand Banks, which are predominantly geostrophic and will contaminate synoptic measurements.

Several of the current meter studies along the slope in this region have demonstrated that the dominant variability in the deep flow can be explained as bottom trapped TRWs (e.g. Thompson, 1977; Johns and Watts, 1986). These are transverse waves whose velocity fluctuations are oriented slanted across the bottom topography; their energy decreases with increasing height off the bottom because of the increased stratification. In an accurate measurement of the mean flow, evidence of the TRWs will vanish such as in the temporal mean vectors in Figure 1 revealing the mean DWBC. Care must be taken, however, when interpreting the variability in such deep current records, and because of the large TRW signal very little is actually known about the true variability of the DWBC.

This paper presents results from an array of bottom current meters across the continental slope at Cape Hatteras intended to measure the deep flow beneath the Gulf Stream, including the DWBC. An associated array of inverted echo sounders surrounding the current meters concurrently monitored the upper layer Gulf Stream path. We show that most of the variability in the deep flow is due to topographic waves, though interestingly the signal is dominated by an energetic 40 day TRW whose characteristics agree with those predicted by topographic wave theory. Because of this dominance we have devised a spatial averaging method to compute the deep cross-stream averaged current so that the contribution from the 40d TRW is minimized at each point in time. The theory behind this is simply that the wave fluctuations averaged across the wavelength do not contribute to the net equatorward flow of water. We optimally weight the individual deep current meter records in order to determine the average current over the wavelength of the 40 day TRW.

This "filtering" leaves behind any other current variance in the 40 day band that has wavelength other than the TRW; we presume that these remaining fluctuations are associated with variations in the strength and position of the DWBC. We then show that the spatially averaged DWBC variability is different in character than that observed by the individual current meters; most notably the fluctuations are oriented nearly along the topography. At periods shorter than 40 days the DWBC variability is somewhat more pronounced relative to the topographic wave signal. Finally, we examine the relationship between the observed deep flow and the upper layer Gulf Stream as measured by the inverted echo sounders. This analysis reveals that the Gulf Stream has some direct influence on the deep flow even in the presence of the topographic waves. In addition, a correlation is found between the orientation of the Gulf Stream path and variations in the DWBC, and we show that this is consistent with simple vorticity constraints.

2. The topographic wave signal

The array of bottom current meters (CMs) and inverted echo sounders (IESs) at Cape Hatteras is shown in Figure 2. Five CMs were deployed in the array, each 100 m off the bottom (one of the moorings failed to release, however). The numbering scheme

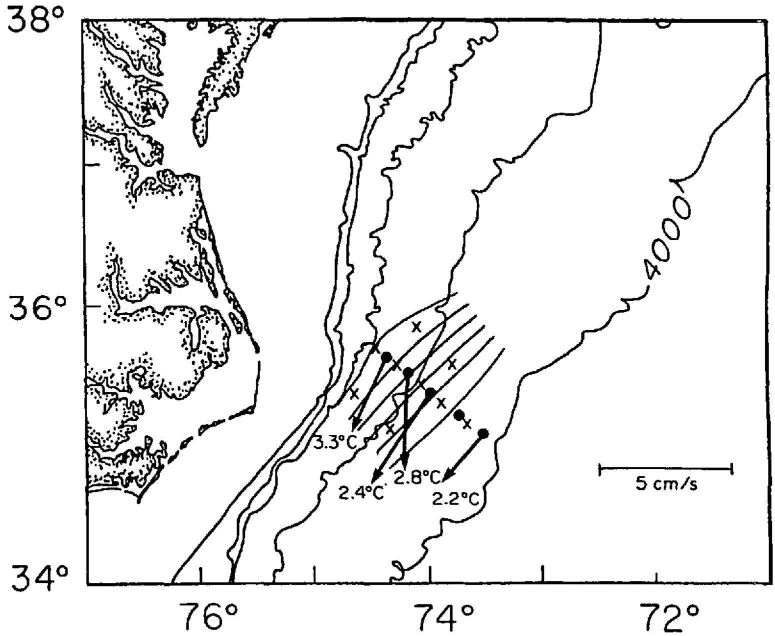

Figure 2. Location of deep current meters (●) and inverted echo sounders (×) at Cape Hatteras, comprising the SYNOP Inlet Array. The current meters are 100 m off the bottom; instruments are numbered 1 to 5 with 1 being onshore. The mean 8-month vectors are shown in relation to the mean Gulf Stream thermocline topography (thin lines) as measured by the inverted echo sounders. Mean temperatures at the current meters are indicated as well.

is such that instrument CM1 is farthest onshore, instrument CM5 is farthest offshore. The instrumentation is part of the Gulf Stream Synoptic Ocean Prediction experiment (SYNOP) which also includes two simultaneous moored programs farther downstream. We refer to the Cape Hatteras array as the Inlet Array, since it is located where the Gulf Stream first enters the interior basin. We report hereeron the first 8-month deployment from November 1987 to June 1988. The IESs continually map the thermocline topography of the Gulf Stream; its mean thermal structure during the deployment period is included in Figure 2. Using the three lines of IESs, time series of position, angle and curvature of the Gulf Stream front are obtained. The closely spaced central line of IESs enables determination of the detailed cross-stream thermal structure of the Gulf Stream (see Cronin and Watts, 1989; Pickart and Watts, 1990).

The mean current vectors and *in situ* temperatures are shown in Figure 2: the flow is everywhere to the southwest indicative of the DWBC flowing under the Gulf Stream. According to its temperature (warmer than 3°C) CM1 is near the transition between Norwegian-Greenland Sea overflow water and the above lying Labrador Sea water. Though it is also considered part of the DWBC, the Labrador Sea water is generally believed to be progressing equatorward at a slower rate than the deeper overflow water.

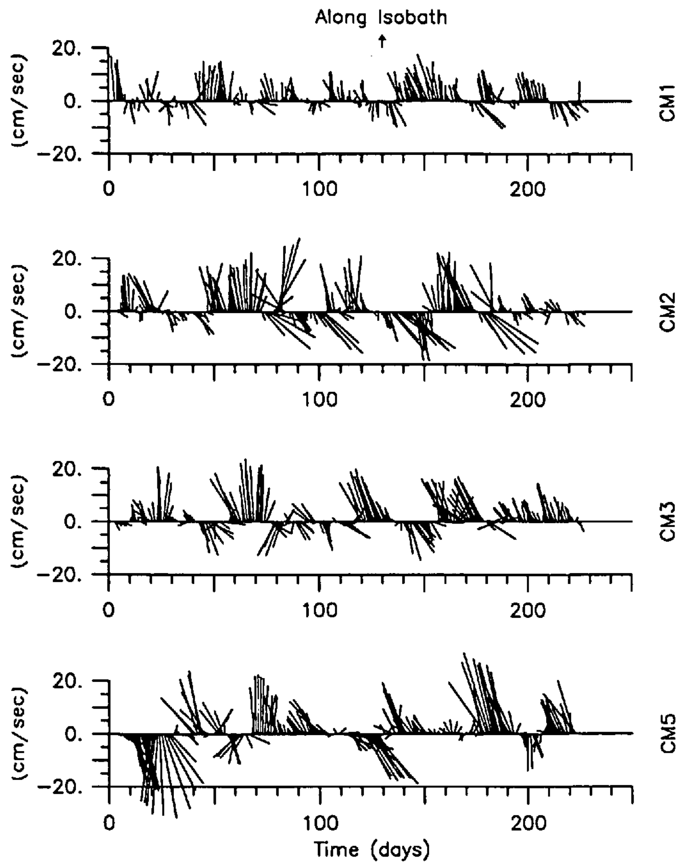

Figure 3. 40 hr lowpassed rotated currents at each of the CM sites, sub-sampled once per day. Positive is to the southwest along the bathymetry (212°T). Day 1 corresponds to 14 October 1987.

For all of the CMs the standard deviations were larger than the means. The topography in this location is oriented roughly at 212°T, and correspondingly we computed currents in a rotated system of along isobath ($+u'$ = 212°T southwest) and cross isobath ($+v'$ = 122°T downslope). The 8-month daily vector stick plots of the rotated currents are shown in Figure 3; there are periodic flow reversals to the northeast (negative) at each of the sites throughout the record, and we show below that these are most likely due to TRWs.

The presence of TRWs along the continental slope between the Grand Banks and Cape Hatteras is now well established. TRWs with periods ranging from 8 days to 64 days have been measured by numerous moored studies, and for the most part their behavior agrees nicely with topographic wave theory (see for example Thompson and Luyten, 1976; Hogg, 1981; Johns and Watts, 1986). The restoring force of a topographic wave is due to the vorticity which is induced as the fluid column crosses the

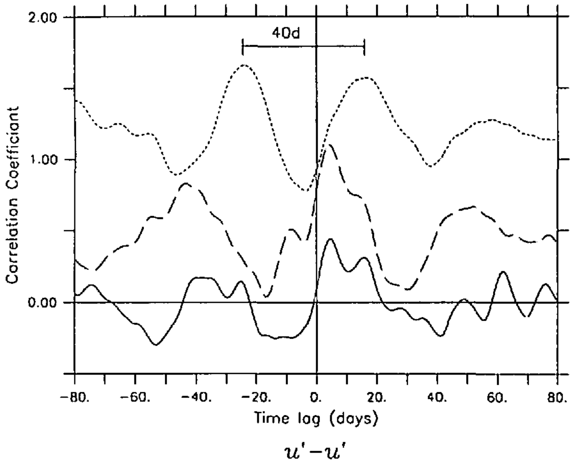

Figure 4. Cross-correlations of alongslope velocity (u') between CM1 and CM2 (solid line), CM2 and CM3 (large dashes), and CM3 and CM5 (small dashes). The dashed lines have been offset by .5 and 1.2 respectively for clarity.

sloping topography and is either stretched or squished (see Pedlosky, 1979). Consequently the transverse motions of the waves are observed to change from nearly along-slope in the low frequency limit (weak restoring force) to a cross-slope orientation at higher frequencies (strong restoring force). The phase propagates down slope, as is required by theory for an offshore energy source, and the waves have vertical trapping scales on the order of 2 km (see Johns and Watts, 1986). It is believed that much of the TRW energy observed along the slope has been remotely generated by the Gulf Stream and subsequently propagated westward. Possible generation mechanisms include large Gulf Stream meanders (Schultz, 1987) and Gulf Stream–ring interactions (Louis and Smith, 1982).

Based on these historical measurements we should expect to see evidence of TRWs in the bottom current meter records from the Cape Hatteras Inlet array. Johns and Watts (1986) have shown that in this region the high frequency cutoff for TRWs is ~8 days. They found that at periods longer than this TRWs dominate the observed deep current variability and are not correlated with local Gulf Stream meandering. At shorter periods, however, the deep fluctuations appear to be coupled with movements of the Gulf Stream front. The moored array in Figure 2 is thus in a region of especially interesting and complex dynamics. The Gulf Stream shifts back and forth within the array, possibly extending to the bottom at times (see Johns and Watts, 1986; Hall, 1986), the DWBC flows underneath, and TRWs propagate through the array presumably having been generated from the Gulf Stream farther east.

a. 40 day wave. To investigate the periodic flow reversals in the stick plots (Fig. 3) we first computed cross-correlations of velocity between the current meter sites. Figure 4

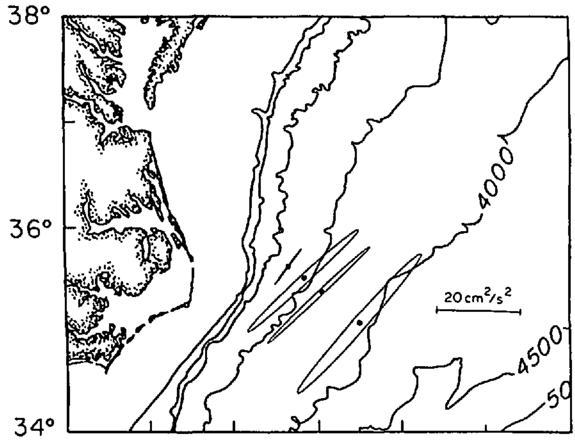

Figure 5. Principle axis variance ellipses at the 40 day period.

shows the lagged $u' - u'$ cross-correlations between the neighboring pairs of CMs. The striking feature in the figure is the sinusoidal character of each correlation curve with a period of roughly 40 days. In each case the offshore CM lags the onshore one; the two onshore pairs have roughly the same lag (6–8 days), and the offshore pair has twice that lag (~16 days, but with twice the instrument spacing). This result implies consistent down-slope phase propagation of a dominant 40 day disturbance.

To document that this 40 day signal is indeed a TRW we compared its characteristics to those predicted by topographic wave theory, and to the various historical measurements. To perform a frequency domain analysis we divided our 8-month time series up into 72 day segments, enabling us to consider a 36 day band for this analysis (from here on we refer to this band as the 40 day band, since it is as close as we can come to resolving the 40 day period). Figure 5 shows the 40 day principle axis variance ellipses at each of the CM sites. They are all very elongated (consistent with transverse motions) and oriented with a slight cross-slope component. Note the sharp decrease in 40 day energy at the farthest onshore site (this is evident as well from inspection of the individual stick plots in Figure 3). Interestingly, the ellipses in Figure 5 are more elongated than those in the 10-64d band of Schultz (1987) and the 12-48d band of Johns and Watts (1986), both of which apply to measurements 500 m off the bottom (compared to 100 m off the bottom here).

The variance ellipses in Figure 5 imply that the wave vector lies along ~134°T (i.e. perpendicular to the average ellipse orientation) which means an orientation angle of $\theta = 11.5°$ from downslope. We then calculated the phase speed of the 40 day wave as follows, $c_p = (1/T)(360/\bar{\phi})(\overline{\Delta s}/\cos(\Delta))$, where T = wave period, $\bar{\phi}$ = average phase offset (=65.5°), Δ = relative angle between mooring line and wave vector (=3.5°), and $\overline{\Delta s}$ = average instrument spacing (=24 km). The resultant phase speed is ~3.6 km/day, which implies a wavelength ($\lambda = c_pT$) of 130 km. The biggest source of error in calculating c_p is the uncertainty in the phase offset $\overline{\phi}$ determined from the spectral analysis, which in our case is ±8.6°. This leads to an uncertainty of ±.47 km/day in the phase speed, or an uncertainty of ±17.0 km in the calculated wavelength. In contrast to $\lambda = 130$ km which we measure here, Thompson (1977) measured a wavelength of 230 km in the 32 day band at 70W (roughly 500 km to the northeast of our array), and Johns and Watts (1986) computed a wavelength of 220 km in the same band at 73.5W (100 km to the northeast).

It is of interest to compare our observed orientation angle θ with that predicted from theory. For a bottom slope of .014 and water depth of 3000 m, the value of topographic β is roughly an order of magnitude larger than planetary β. The dispersion relation for topographic Rossby waves in a stratified ocean neglecting planetary vorticity (Pedlosky, 1979) can be written,

$$T = \frac{2\pi \tanh(2\pi ND/\lambda f_0)}{N\Gamma \sin\theta} \tag{1}$$

where T = period, λ = wavelength, N = Brunt-Väisälä frequency (constant), D = characteristic water depth, f_0 = Coriolis parameter, Γ = bottom slope, and θ = orientation angle from downslope. Using the measured values of T and λ we can use (1) to compute a predicted orientation angle, which we then compare to our observed value. The predicted group speed and vertical decay scale can also be calculated. We used the following values for the various parameters in (1): $\Gamma = .014$, $f_0 = 8.5 \times 10^{-5}\ \mathrm{sec}^{-1}$, $D = 3000$ m, and $N = 10^{-3}\ \mathrm{sec}^{-1}$ (typical deep water value in this region). For these values the ratio $2\pi ND/\lambda f_0 = 1.7$ and correspondingly (1) is simplified as $\tanh(2\pi ND/\lambda f_0) \sim 1$ (i.e. the short wave/large stratification limit applies and explicit dependence on the wavelength drops out). The resulting predicted orientation angle, $\theta = \sin^{-1}(2\pi/N\Gamma T)$, is 8.3° which compares reasonably well with our measured value of 11.5° (it is worth noting that there is uncertainty as well in determining the appropriate angle of the isobaths from Figure 2).

We thus have the following scenario regarding the fluctuations observed by the bottom current meters, as depicted in Figure 6: A 40 day topographic wave, which dominates the observed variability and has a wavelength of 130 km, propagates its phase at 3.6 km/day at an angle of 11.5° from downslope (prediction = 8.3°). The predicted vertical decay scale is 1700 m, and the predicted group speed is 25.6 km/day. The group is progressing to the southwest (upslope) at 231°T presumably having come from downstream in the Gulf Stream. At this point it is unclear why the current records contain such a distinct 40 day disturbance; further study will be required to investigate its origin. In any event it will be interesting to see if the 40 day waves persist for the entire 3 year length of the array deployment.

b. Higher frequency variability. As mentioned above, TRWs have been measured along this region of the continental slope over a range of frequencies, the high

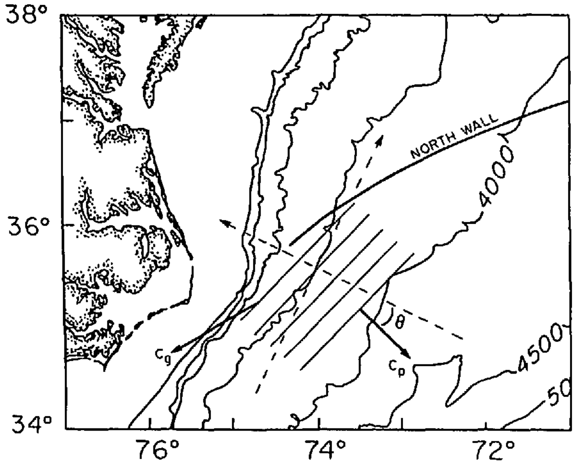

Figure 6. Schematic of the 40 day topographic Rossby wave. The wave crests propagate downslope at the angle θ while the group progresses upslope to the southwest. The historical position of the Gulf Stream north wall is shown for comparison.

frequency cutoff occurring near 8 days. In our records the u' (along isobath) variance is peaked at the 40 day band, indicating that the topographic wave signal is not as pronounced at very long periods. This was found to be true as well at other locations. For example Schultz (1987) found more energy in the 32d band than the 64d band in deep current records downstream of Cape Hatteras. In addition, the increase in energy with depth which is characteristic of bottom trapped TRWs was present at 32 days but not at 64 days. Near 62W Welsh *et al.* (1989) also found a decrease in deep energy along the slope at periods greater than 30 days.

One of the observational signatures of TRWs is the turning of the principle axis ellipse to a more cross-isobath orientation at higher frequencies. This was illustrated nicely by Thompson and Luyten (1976) who analyzed data from a single mooring at 70W. They found that the change in orientation of the principle axis ellipse versus frequency agreed quite well with that predicted from theory (Fig. 7a). We made the same comparison with our data, plotting the average orientation angle of the four current meters as a function of frequency, compared to that predicted using the dispersion relation (1). In sharp contrast to Thompson and Luyten's (1976) results we see no consistent turning of the ellipse (Fig. 7b).

A review of the existing literature on TRWs reveals that the observed rotation of the ellipse with frequency often does not conform to that predicted by theory, and in fact the agreement in Figure 7a is the exception rather than the rule. While the ellipses in general are found to rotate with the correct sense over large changes in period (for instance in our data they turn more across the topography for periods less than 13 days), the observed scatter is substantial (see for example Johns and Watts, 1986; Schultz, 1987; Thompson, 1977). Whether these discrepancies result from uncertain-

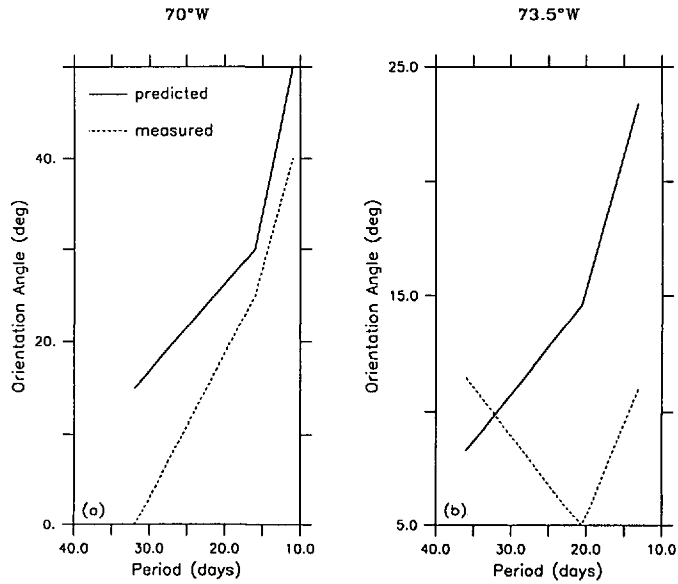

Figure 7. Orientation angle of the principle axis of variance (measured from alongslope) as a function of period, for that observed (dashed line) versus that predicted from topographic wave theory (solid line). (a) Comparison at 70W using data from a single mooring (from Thompson and Luyten, 1976). (b) Comparison at the Cape Hatteras Inlet Array using the average observed angle at the four sites.

ties in the spectral techniques or from real oceanic deviations remains to be determined. Johns and Watts (1986) attributed an unexpectedly large cross-isobath orientation of deep fluctuations in the 14 day band to meandering of the deep Gulf Stream. In Figure 7b it is seen that the higher frequency fluctuations in our records are oriented more alongslope than expected; below we offer a possible explanation for this, namely that it is due to variability of the DWBC.

3. Variability of the DWBC

The results of the previous section demonstrate that the dominant variability in the individual bottom current meter records is due to a 40 day topographic wave propagating through the array. The mean temperatures in Figure 1 indicate, however, that the four instruments spanned the DWBC as well. The mean current vectors in Figure 1, which should be void of any wave influence, do indeed point to the southwest; however, the temporal variability of the DWBC itself is effectively masked by the topographic wave signal.

The waves of course do not have any net transport equatorward as does the DWBC. At a given current meter site the wave transport vanishes in the long term temporal mean, and at each moment in time there is also no net wave transport over an integral number of wavelengths. If the spacing of current meters were fine enough and the mooring line very long then we could easily sum up the velocity over a number of wavelengths and the wave signal would identically vanish (assuming that the wave has a constant amplitude over this distance). The separation between the farthest onshore and farthest offshore current meters in our array is approximately 100 km (Fig. 1) which is roughly three-quarters of the wavelength of the 40 day TRW. Below we show how to use these four current meters to optimally estimate the average velocity over a single wavelength, thereby reducing the wave signal and revealing the DWBC variability.

a. Optimal weighting. We are interested in integrating our current meter measurements across-stream to calculate the average velocity of the DWBC over the distance λ, a single wavelength of the 40 day TRW. At a given current meter site, i, the component of velocity associated with the wave is

$$u_i(t) = A\sin(2\pi t/T + \phi_i), \tag{2}$$

where A = wave amplitude and ϕ_i is the phase lag (known from the observations). The transport per unit height is $\sum_{i=1}^{4} L_i u_i(t)$, where the L_i's are cross-stream lengths such that $\sum_{i=1}^{4} L_i = \lambda$. Normalizing the transport by λ gives the average velocity over the wavelength in terms of the (as yet unknown) weights w_i,

$$\overline{u}(t) = \sum_{i=1}^{4} w_i u_i(t), \tag{3a}$$

$$\sum_{i=1}^{4} w_i = 1, \tag{3b}$$

where $w_i = L_i/\lambda$. Inserting (2) into (3a) then re-arranging gives

$$\overline{u}(t) = \hat{A}\sin(2\pi t/T + \hat{\phi}) \tag{4}$$

where

$$\hat{A} = A\sqrt{\left(\sum_{i=1}^{4} w_i \cos(\phi_i)\right)^2 + \left(\sum_{i=1}^{4} w_i \sin(\phi_i)\right)^2}$$

and

$$\hat{\phi} = \tan^{-1}\left(\frac{\sum_{i=1}^{4} w_i \sin(\phi_i)}{\sum_{i=1}^{4} w_i \cos(\phi_i)}\right).$$

We want to determine the (nonzero) weights such that $|\overline{u}(t)|$ is minimum; in

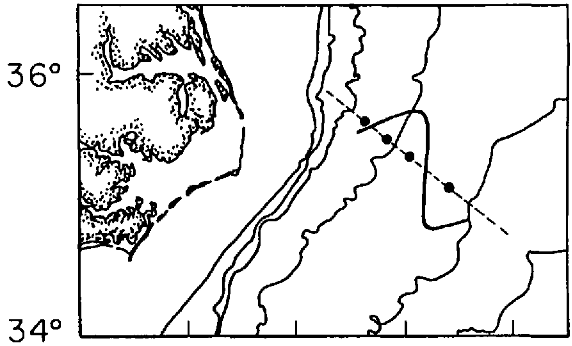

Figure 8. Schematic showing the 130 km wavelength of the 40 day topographic wave in relation to the four bottom current meters.

particular find the w_i's which satisfy

$$(\partial/\partial w_i \hat{A} = 0)_{i=1,4}, \tag{5}$$

subject as well to the constraint (3b) (note that the weights are independent of time). It is the case, however, that (3b) does not ensure that each individual weight be positive, which is required for a physical result. Thus we must constrain the system further. The next simplest step is to split the integration into two sections, i.e. use a subset of current meters to estimate the velocity over one half of the wave, and use the remaining current meters to estimate the velocity over the other half of the wave (which results in two average velocities 180° out of phase). It is then a matter of specifying the two subsets.

Figure 8 shows the spacing of bottom current meters in relation to the wavelength of the 40 day TRW. It is evident that we should use instruments CM1 and CM5 to estimate the average wave velocity over one half of the wavelength, and CM2 and CM3 to estimate the velocity over the other half-wavelength (this is true regardless of the phase of the wave). This results in the additional constraints

$$\begin{aligned} w_1 + w_4 &= .5 \\ w_2 + w_3 &= .5, \end{aligned} \tag{6}$$

which are more stringent than (and replace) (3b).

The conditions (5) and (6) result in a matrix system for the w_i's,

$$A\mathbf{w} = \mathbf{b} \tag{7}$$

where $A_{ij} = \cos(\phi_i + \phi_j)$ for $i = 1,4$ and $j = 1,4$; $A_{51} = A_{54} = A_{62} = A_{63} = 1$; $A_{52} = A_{53} = A_{61} = A_{64} = 0$; and $\mathbf{b} = (0, 0, 0, 0, .5, .5)$. The system (7) is over determined and as such has no exact solution. However the "best approximation" is that which minimizes the difference $|A\mathbf{w} - \mathbf{b}|$, which is a matter of finding the $\mathbf{w}$ which satisfies the expression

$$(A^TA)\,\mathbf{w} = A^T\mathbf{b}, \tag{8}$$

provided (A^TA) has an inverse.

Using the values of ϕ_i determined from the spectral analysis (i.e. the phase lags at the 40 day period: $\phi_1 = 0°$, $\phi_2 = 80°$, $\phi_3 = 130°$, $\phi_4 = 263°$), the solution to (8) was determined numerically giving the following values of the weights: $w_1 = .0581$, $w_2 = .2630$, $w_3 = .2370$ and $w_4 = .4419$. In light of Figure 8 this is just the result expected, i.e. the wave velocity over one half of the wavelength is roughly the average of CM2 and CM3 ($w_2, w_3 \sim 1/4$), and the velocity over the other half-wavelength is given mostly by CM5 ($w_4 \sim 1/2$, $w_1 \sim 0$).

When these weights are inserted into (4) the resulting amplitude $\hat{A}$ of the average velocity is $(4 \times 10^{-6})\,A$, i.e. a reduction of more than 99.9% of the TRW amplitude A. Thus for a plane wave with wavelength = 130 km, using the above weights should substantially reduce the wave signal and reveal the average DWBC velocity over that distance. If there is a significant change in amplitude of the topographic wave signal over the length of the array, this can be accounted for by making the amplitude A in (2) a function of current meter site. In our case the principle axis variance at 40 days (Fig. 5) is roughly equal at the three offshore sites used to calculate the average velocity ($w_1 \sim 0$), so we need not consider a varying A.

This weighted average is designed to remove the topographic wave variance at the 40 day period (i.e. remove the coherent signal associated with the observed phase offsets). Any other variance at 40 days (explicitly that of the DWBC) is left behind, as is the topographic wave variance at other periods. If the dominant TRW signal described above happens to undergo a change in period at some point during the record then the averaging scheme will allow this portion of the signal to remain. This does not mean however that the filter has failed; the topographic wave contribution at 40 days, no matter how small, will continue to be minimized. To get an idea of how much the dominant TRW signal actually does change period we did a set of linear least squared fits of sines and cosines to the time series of u' at CM5. Five periods were used in each fit, spanning a different range of periods in each case from $\Delta T = 1$ day to $\Delta T = 20$ days (all centered at $T = 40$ days). Each fitted series was then compared against the 30 day low passed time series of u' and the respective correlation coefficient γ computed. It turns out that the best fit occurs for $\Delta T = 2$ days (with a $\gamma = .70$). This is further evidence that the dominant TRW signal persisted near 40 days throughout the record. It should be noted that even with the 40 day weights, a TRW that undergoes a change in period of $\Delta T = 2$ days will still have its amplitude in (4) reduced by 93%.

b. Spatially averaged time series. The technique described above can be applied to remove the wave signal at any given period. We computed the optimal set of weights for three different periods: 40 days ($\lambda = 130$ km), 20 days ($\lambda = 98$ km) and 13 days

Table 1. Optimal weights used to remove the topographic wave signal from the cross-stream averaged velocity at 40 days, 20 days and 13 days. Each set of weights was determined by numerically solving (7).

	w_1	w_2	w_3	w_4
40 day	.0581	.2630	.2370	.4419
20 day	.2308	.0045	.4955	.2692
13 day	.2547	.0002	.4998	.2453

($\lambda = 95$ km). The corresponding weights are listed in Table 1. The time series of spatially averaged velocity with the 40 day TRW removed (but other 40 day variance remaining) is shown in Figure 9. Although the record still contains wave variance from other periods, the dominant TRW signal is the 40 day wave whose u' (along isobath) variance is more than twice that in the 20 day and 13 day bands. In addition, the remaining wave variance in the two higher frequency bands is itself reduced by more than 60% when the 40 day weights are used. To document that the time series in Figure 9 is not dominated by a wave-like process (as were the individual current meter records) we computed its u' lagged auto-correlation and compared it to that for CM5 (Fig. 10). As seen in the figure CM5 (along with the other CMs as well) shows a negative peak at ± 20 days and a positive peak at ± 40 days (i.e. the 40 day TRW signal), whereas the auto-correlation of the average velocity falls off steadily with no such oscillations.

The time series in Figure 9 shows more consistent flow to the southwest than do the individual current meter records (compare to Fig. 3). Note, however, that there are still reversals to the northeast, though they are sporadic and generally weak (the exception

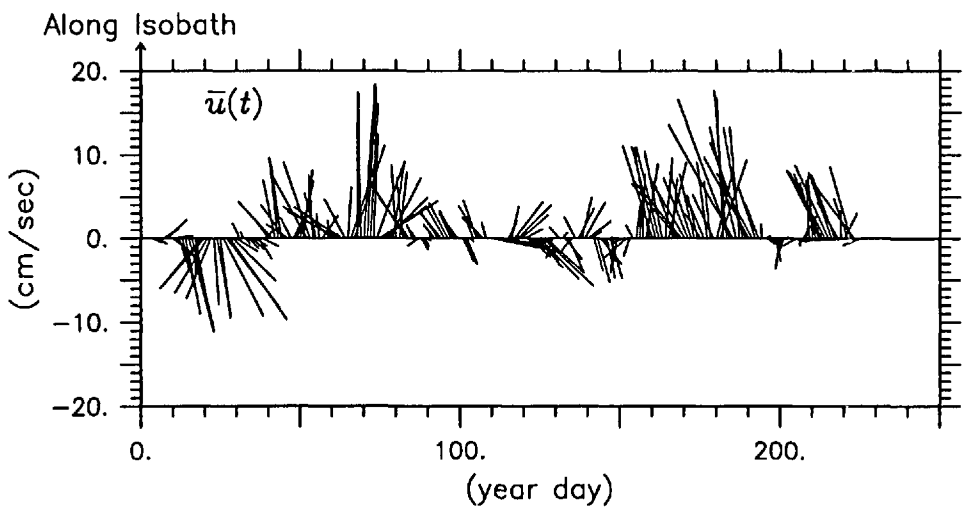

Figure 9. Vector stick plot of average velocity, $\bar{u}(t)$, computed using the 40 day weights in Table 1. Positive is to the southwest along the bathymetry; day 1 corresponds to 14 October 1987.

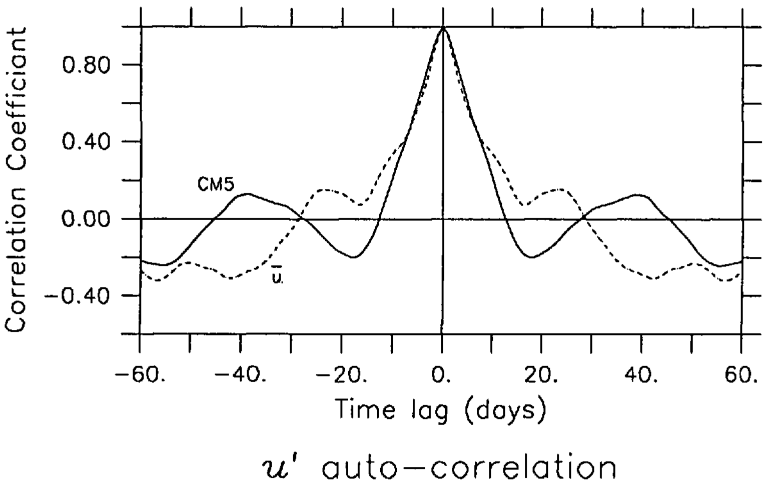

Figure 10. Auto-correlation of alongstream velocity versus time lag for CM5 compared with that for the average velocity.

to this is the anomalous event at the beginning of the record, which upon close inspection is seen to occur only at the offshore-most site (see Fig. 3) and contains the strongest northeast velocities recorded at any of the sites). In Figure 11 we plot the average velocity principle axis ellipses at the three periods and compare them to the mean of the individual CM principle axis ellipses. For each period the calculation was done using the weighted average time series with that period's wave signal removed (using the appropriate weights in Table 1). In so far as the spatially averaged current reflects the DWBC variability, it is seen that in contrast to the topographic waves, fluctuations of the deep boundary current are aligned more along the topography (though somewhat downslope at 40 days). Note that the biggest difference in magnitude between the wave and average velocity ellipses occurs at the 40 day period. This suggests that the TRWs do not dominate the DWBC fluctuations as much at shorter periods, which might help explain why the higher frequency ellipses referred to earlier (Fig. 7) are aligned more along the topography than expected from wave theory.

4. Relationship of the Gulf Stream to the deep flow

The other component of the Cape Hatteras Inlet moored experiment is the array of 9 IESs surrounding the line of deep current meters (Fig. 2). The IESs enable us to measure various features of the upper layer Gulf Stream, and provide the opportunity to explore possible dynamical links between the deep flow—including the TRWs and DWBC—and the Gulf Stream.The bottom mounted IES is able to accurately measure the local depth of a given isotherm (say 12°C) of the Gulf Stream as a function of time (see Watts and Johns, 1982). Using this information at all the sites a daily objective analysis (OA) map of the Gulf Stream 12°C topography can be generated following

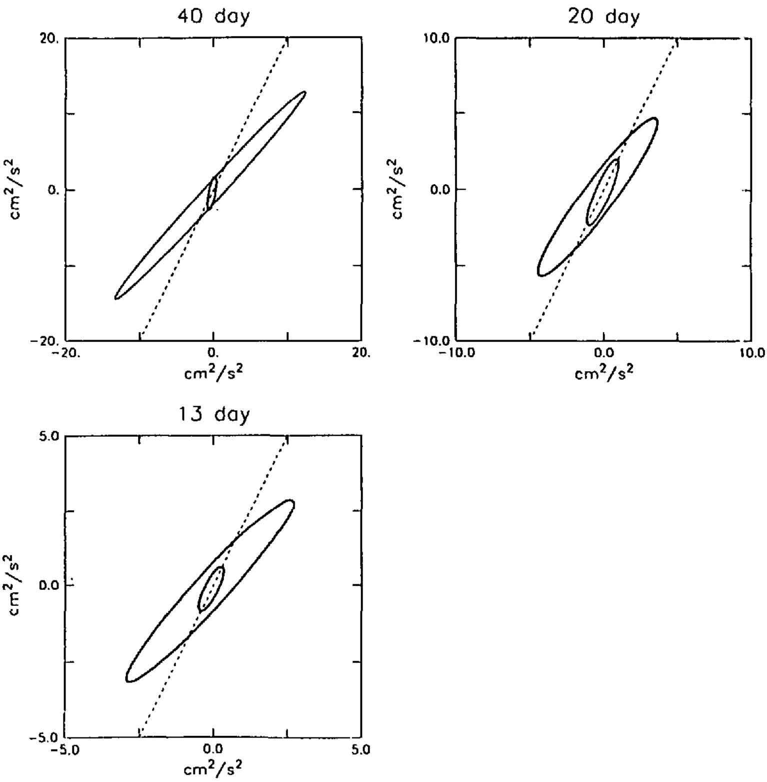

Figure 11. Principle axis variance ellipses in relation to the bottom topography (dashed line) at three different periods. The large ellipse is the mean of the four individual CM variance ellipses, indicative of the topographic waves. The small ellipse is that of the spatially averaged velocity computed using the appropriate set of weights from Table 1, indicative of the DWBC.

the procedure of Watts *et al.* (1989) (Fig. 12a). From this collection of OA maps we generated time series of Gulf Stream displacement (i.e. lateral displacement of the 450 m contour in Figure 12a) and offshore angle of the Gulf Stream. In addition, a time series of path curvature was computed by fitting a bi-cubic spline to the 450 m contour of the OA maps.

The 30 day lowpassed curves of Gulf Stream displacement (D), angle (α) and curvature (κ) are shown in Figures 12b and 12c. Displacement is measured relative to the onshore IES, with positive being offshore. Angle refers to the average angle of the Gulf Stream over the length of the IES array (~100 km; values reported are relative to the alongstream axis of the array, with positive implying offshore orientation). It is seen in Figure 12b that the curvature and displacement are very highly correlated, with offshore displacements associated with meander troughs and vice versa. Note that the curvature is negative for most of the record (in fact only during the farthest offshore meander does it become positive); this is consistent with the mean path of the Gulf Stream in this region where it is separating from the boundary and turning offshore.

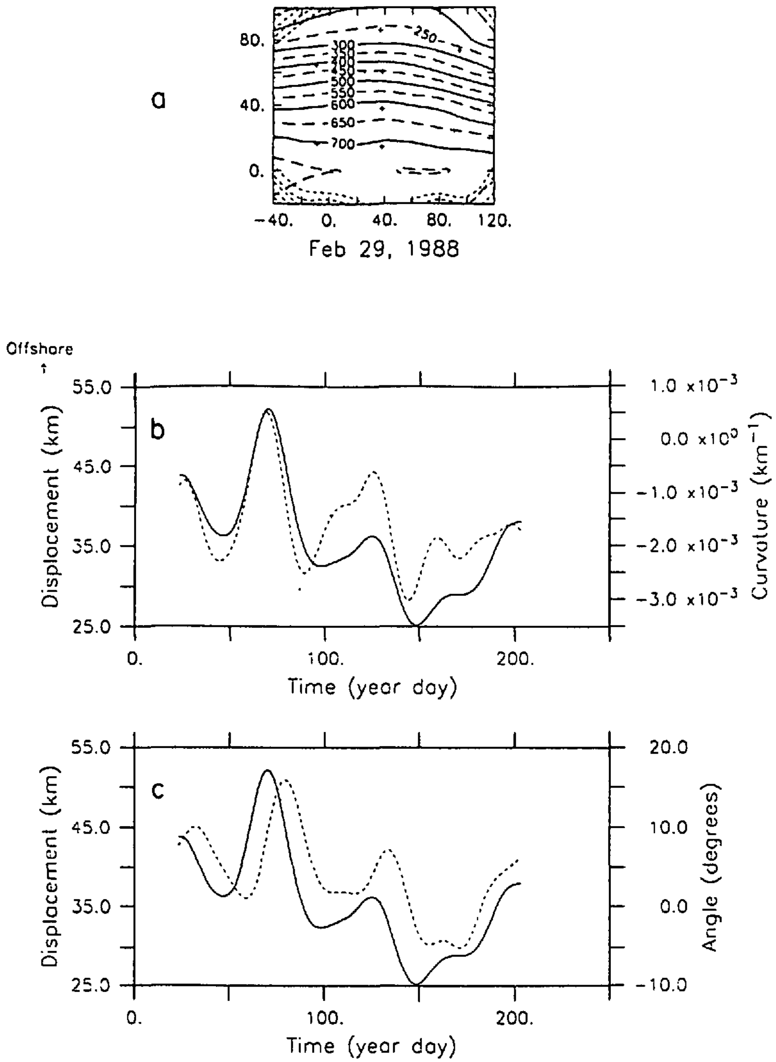

Figure 12. (a) Objective Analysis (OA) map of the Gulf Stream 12°C topography for a particular day during the 8-month deployment. Contours are in meters (the dashed regions near the edges represent more than 20% error). (b) 30 day lowpassed time series of onshore/offshore Gulf Stream displacement (solid line) and path curvature (dashed line) computed using the 450 m contour of the daily OA maps. Day 1 corresponds to 14 October 1987. (c) Same as (b) but comparing onshore/offshore displacement to path angle (dashed line).

The angle of the Gulf Stream path is also highly correlated with displacement (Fig. 12c), except that it lags the displacement by approximately 8–10 days.These results can be understood by noting that the meander envelope of the Gulf Stream at Cape Hatteras is quite small and the path does not undergo large convoluted meanders that

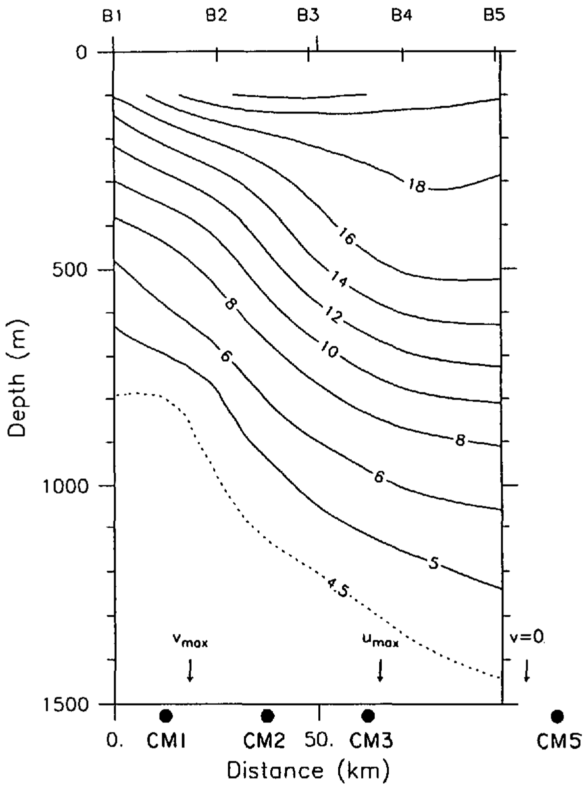

Figure 13. 8-month mean vertical section of temperature at the CM mooring line, computed using IESs B1 through B5. The cross-stream locations of the bottom CMs are indicated below the section. Also shown is the mean position of maximum deep (>1500 m) inflow to the Gulf Stream (v_{max}), maximum deep alongstream flow (u_{max}) and zero deep inflow ($v = 0$), from the 73°W PEGASUS experiment (Halkin, *et al.*, 1985).

are characteristic farther downstream. For the simple sine-wave-like disturbances observed at Cape Hatteras one would expect D and κ to be well correlated and in phase, while D and α should be in quadrature with D leading. A spectral analysis of the 40 hr lowpassed D, κ and α records (not shown) reveals that at all periods greater than 5 days D and κ have significant coherence and are approximately in phase, while D coherently leads α with an average phase offset of 60.5°. The 8–10 day lag observed in the 30 day lowpassed curves of Figure 12c is roughly one-quarter of the energetic 40 day period.

Pickart and Watts (1990) have recently demonstrated that the IES can also accurately measure the local vertical profile of temperature through the main thermocline as a function of time, for regions of the Gulf Stream where meandering is small. This is based on the assumption that the predominant variability is first baroclinic mode. We applied their methodology to compute an average vertical section of temperature along the central IES line, which is shown in Figure 13 in relation to the placement of the bottom current meters. It is seen that CM2 is located directly beneath the sharpest part of the Gulf Stream front. It should be noted that the standard deviation meander width of the Gulf Stream during the 8-month deployment period was less than 10 km. Below we investigate the cross-stream structure of the deep fluctuations in relation to the upper layer Gulf Stream as pictured in Figure 13.

a. The deep components of flow. Does the Gulf Stream reach the bottom at Cape Hatteras? Farther downstream it has been demonstrated that the Gulf Stream clearly does extend to the bottom on the basis of its vertically coherent fluctuations (see Hall, 1986; Welsh *et al.*, 1989). Figure 2 shows that, in the mean, the Gulf Stream does not penetrate to the bottom here, rather the DWBC crosses under the Gulf Stream flowing to the southwest. We show below, however, that the Gulf Stream does continually influence the deep flow at this location and occasionally its northeast flow does extend to the bottom.

Recent modelling results have demonstrated that the Gulf Stream and DWBC may dynamically influence one another at Cape Hatteras where the two currents cross. Hogg and Stommel (1985) argued that the DWBC should move to deeper depths upon crossing under the Gulf Stream in order to maintain a constant layer thickness. Thompson and Schmitz (1989) showed that when the magnitude of the DWBC is increased in a two layer primitive equation numerical model, the upper layer Gulf Stream separates from the continental boundary at a lower latitude and subsequently undergoes more pronounced meandering downstream of the crossover. Comparing deep PEGASUS velocity data and concurrent satellite SST maps, Leaman (1989) observed a relationship between the strength of the DWBC and meander characteristics of the Gulf Stream consistent with Thompson and Schmitz's (1989) model results. To investigate the relationship of the Gulf Stream to the deep flow in our data set we computed cross-correlations at the 40 day period between u', v', T as measured by the deep current meters, and D and α computed from the IESs. A summary of the resulting coherences and phases appears in Table 2, which we now discuss.

The first four columns of Table 2 correspond to the four bottom current meters, each of which includes the strong topographic wave signal as discussed above. The last column, denoted by Σ, corresponds to the time series of spatially averaged velocity which is void of the 40 day TRW signal and therefore represents predominantly DWBC variance at this period. In the top panel we correlate the alongslope velocity and cross-slope velocity at each site. For a transverse topographic wave we expect that these two variables should be highly correlated and $\sim$180° out of phase (equatorward fluctuations coincident with upslope fluctuations). This is the case as expected at each of the CM sites; however, it is seen that the averaged u' and v' are uncorrelated, giving further confidence that the wave signal has been successfully removed. The second panel correlates downslope velocity and temperature. Thompson (1977) observed that these two variables are $\sim$90° out of phase for TRWs, with upslope flow bringing up

Table 2. Summary of coherences and phases at the 40 day period between different variables measured by the current meters (u' = alongslope velocity 212°T, v' = downslope velocity 122°T, T = temperature) and inverted echo sounders (D = onshore/offshore displacement, α = angle). Phases are indicated in parentheses. Only those values which are coherent above the 95% confidence level (.63) are listed. Columns 1–4 correspond to the individual current meters, Σ denotes the spatially averaged velocity.

	CM SITE				
	1	2	3	5	Σ
u', v'	.86 (−157°)	.86 (−167°)	.90 (−168°)	.69 (180°)	—
v', T	—	—	.81 (92°)	.71 (71°)	.87 (113°)
u', D	—	—	.75 (9°)	.65 (−112°)	.74 (−53°)
v', D	.71 (−61°)	—	—	—	—
T, D	—	.79 (164°)	—	.79 (−64°)	—
u', α	—	—	—	—	.68 (32°)
v', α	—	—	—	—	.65 (45°)

95% significance level = .63

colder water and vice versa. We see here that at the offshore sites the two variables are roughly in quadrature, but farther onshore there is no significant correlation. This is consistent in that the individual v' auto-correlations (not shown) reveal that the cross-slope TRW signal is most pronounced offshore. Note as well that the spatial averages are also (strongly) correlated as such, which is perfectly consistent: whether the cross-slope flow originates from a topographic wave or a fluctuation of the DWBC the subsequent effect on temperature will occur either way.

In the third panel we investigate the relationship between the deep flow and the onshore/offshore displacement of the upper layer Gulf Stream. For the alongslope flow (u') the strongest correlation occurs at site 3 where onshore Gulf Stream displacements are in phase with northeast velocity fluctuations. Keep in mind that the alongstream velocity core of the Gulf Stream is offset with depth towards the anti-cyclonic side of the stream. As marked in Figure 13, the location of the deep core below 1500 m according to the 3-year mean PEGASUS velocity section at 73W (Halkin *et al.*, 1985) is just offshore of site 3. CM3 is thus the location of strongest deep Gulf Stream flow, but as seen by the mean vectors of Figure 2 it is also where the DWBC is strongest (i.e. it is the "heart" of the crossover).

The alongslope average velocity Σ is also correlated with Gulf Stream displacement in a similar fashion, only there is a time lag such that northeast velocity fluctuations follow onshore displacements. Inspection of the time series of u' and D (Figs. 9 and 12b) shows that the deep flow here does not actually reverse to the northeast every time the Gulf Stream meanders onshore, but rather the southwest flowing DWBC is usually weakened. Johns and Watts (1986) speculated that only during very large meanders does the Gulf Stream's northeast flow extend to the bottom in the region near Cape Hatteras. This notion is consistent with what we find here in that during the farthest onshore Gulf Stream excursion the spatially averaged deep velocity undergoes its strongest northeast reversal (excluding the above-mentioned anomalous event at CM5), while during the farthest offshore excursion the southwest flow attains its largest value.

The effect of the Gulf Stream on the deep cross-slope flow is quite different than that observed for the alongslope flow. As seen in Table 2 the only significant correlation between v' and D occurs at the onshore-most site, such that downslope flow follows offshore Gulf Stream displacements. This observation can also be understood in the context of Figure 13, which shows that according to the mean PEGASUS section the maximum inflow to the deep Gulf Stream occurs just offshore of site 1 (whereas the maximum inflow from the anti-cyclonic side occurs well offshore of site 5). The temperature correlations tell yet a different story. At site 2 colder temperatures are in phase with offshore displacements, in contrast to no observed correlation at either neighboring site. This is also consistent with Figure 13 which shows that the sharpest part of the Gulf Stream thermal front occurs at site 2; it should be noted that this front is observed to extend to the bottom (e.g. Pickart, 1987) (although at this location any thermal shear associated with the DWBC would be hard to distinguish from the deep Gulf Stream front). Previous work also suggests that, away from the strong front, the Gulf Stream does not influence bottom temperatures at long periods. Johns and Watts (1986) found no significant correlations in the 24–48 day band between thermocline displacements and bottom temperatures at two locations roughly 15 km shoreward and 15 km seaward of the sharpest part of the Gulf Stream front. The additional temperature correlation at site 5 (as well as the weak $u' - D$ correlation at site 5) is curious, and it may be that these are related to the strong anomalous event that occurred at this location. The full three year time series will shed light on this.

The final panels in Table 2 relate the observed deep flow to changes in orientation (α) of the Gulf Stream path. It is seen that there are no significant correlations at any of the individual sites; however, both the alongslope and cross-slope average velocity show weak correlations with changes in Gulf Stream angle. Regarding the alongslope flow, according to Table 2 fluctuations in average velocity lead changes in angle. This most likely is just a consequence of the fact that the Gulf Stream angle is highly correlated to—and lags—Gulf Stream displacement for the sine-wave-like meanders at Cape Hatteras (see Fig. 11c). The dynamically significant cause and effect here is most likely between displacement and alongslope average velocity, especially in light of the $u' - D$ correlation observed at site 3. However, the correlation regarding cross-slope average velocity and angle is much different, for there is no observed relationship between cross-slope average velocity and displacement. The $v' - \alpha$ correlation of Σ in Table 2 implies increased downslope flow associated with increased offshore angle of the Gulf Stream. In the next section we describe how cross-slope flow of the DWBC at Cape Hatteras might be dynamically related to the orientation of the Gulf Stream, and

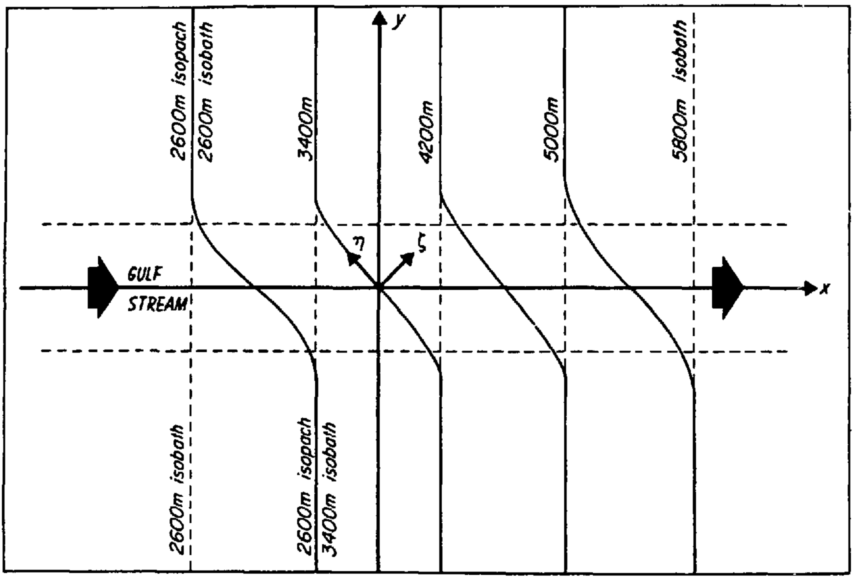

Figure 14. Lines of constant deep layer thickness (solid lines) shown crossing bottom contours (dotted lines) in response to the thermocline of the Gulf Stream (from Hogg and Stommel, 1985).

explain why one might expect such flow to be more sensitive to changes in the angle of the Gulf Stream than to changes in its onshore/offshore position.

b. Cross-slope flow of the DWBC. In Hogg and Stommel's (1985) model of the deep flow near the Gulf Stream they argued that if the DWBC is to maintain its layer thickness upon crossing the Gulf Stream, then it must move downslope to account for the deepening of the main thermocline across the Gulf Stream front. They considered a two layer case in which the deep layer is bounded above by the main thermocline and below by the bottom topography. In their idealized representation the DWBC crosses the (zonal) Gulf Stream at an angle of 90° (Fig. 14). In actuality, the mean path of the Gulf Stream is 40–45°T at this location and the topography is oriented to the southwest at roughly 212°T (Fig. 1), which means that the angle of incidence is in fact small, more like 10–15°. In addition, the slope of the topography significantly decreases with offshore distance.

To investigate if Hogg and Stommel's (1985) proposed scenario is at work in the ocean we computed the deep layer thickness contours which result from a more realistically modelled configuration of the Gulf Stream and bottom topography. We fit a hyperbolic tangent to the 8-month mean thermocline profile in Figure 13 (i.e. to the 12°C isotherm) and fit an exponential to the bottom topography along the central mooring line. This configuration is shown in Figure 15a in relation to the deep current meter sites. Figure 15b shows the resulting isopachs of deep layer thickness with the

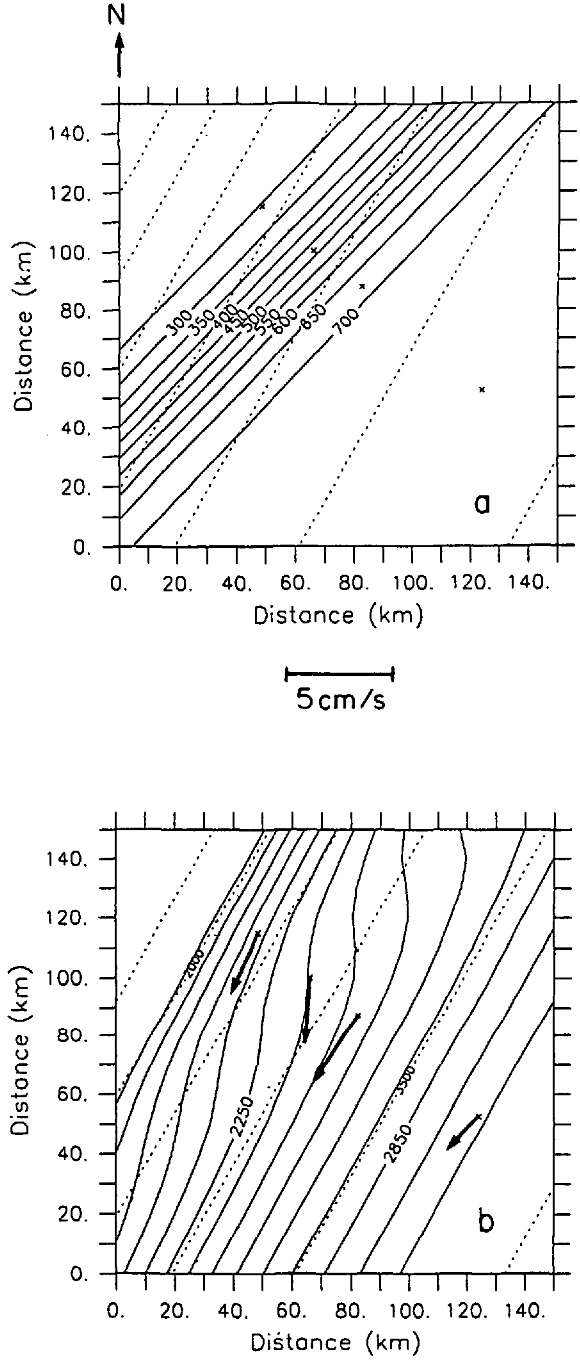

Figure 15. (a) Modelled depth contours of the 12°C surface of the Gulf Stream (solid lines) in relation to the isobaths (dashed lines). The positions of the four CMs are indicated by x's. (b) Lines of constant deep layer thickness that result from the orientation of the Gulf Stream over topography in (a). The 8-month mean CM vectors from Figure 2 are overlayed.

mean current vectors from Figure 2 overlayed. The agreement is striking, suggesting that the DWBC indeed tends to preserve its layer thickness upon crossing under the Gulf Stream. Note in Figure 15b that because the crossover line is not perpendicular to the topography, as in Hogg and Stommel's (1985) schematic, the deeper flow of the DWBC crosses the Gulf Stream (and moves downslope) before the shallower flow does. Thus only at CM2 is the DWBC actually crossing the Gulf Stream in our array; the deeper DWBC flow has already crossed, while the shallower part has yet to cross. Also, note that because the topography is weaker downslope there is a stronger implied cross-slope component of flow there than in the shallower part of the DWBC.

The tendency of the deep flow to preserve its layer thickness (or roughly its potential vorticity since the relative vorticity of the DWBC is weak) can also account for the observed correlation between Gulf Stream angle and downslope flow discussed in the previous section. Figure 16 isolates the effect on downslope flow due to a change in Gulf Stream displacement (top panel) and change in angle (bottom panel). The ranges of displacement and angle in the figure are those observed during the 8-month deployment period. As seen in the top panel, when the Gulf Stream moves offshore (with α constant) the crossover line progresses from site 1 to site 3, causing downslope flow at a single CM site only. When the angle of the Gulf Stream changes, however, the crossover line goes from being non-existent within our model domain (when the DWBC and Gulf Stream are anti-parallel) to a stronger across-slope orientation which leads to downslope flow at sites 2 and 3. Thus, because of the fact that the CMs are aligned directly across the topography, the overall change in the measured cross-stream averaged downslope flow is greater by a factor of 3 for the change in angle than for the change in displacement. This may explain why the average downslope velocity was found to be correlated with changes in Gulf Stream angle but not with changes in displacement. Interestingly, the observed correlation is such that DWBC fluctuations lead changes in Gulf Stream angle, though this needs to be tested further with the longer time series.

5. Summary

Results from an 8-month deployment of deep current meters and inverted echo sounders off Cape Hatteras have revealed some aspects of the complicated nature of the deep flow in this region. The mean velocity vectors all point to the southwest displaying the DWBC in the temperature range of 2.2–3.3°C, with a speed of 3–4 cm/sec. The low frequency variability measured by the individual current meters is dominated, however, by topographic Rossby wave motions, particularly an energetic 40 day wave whose characteristics agree with theory and historical observations. The energy of the 40 day wave propagates up-slope, presumably having originated elsewhere downstream in the Gulf Stream.

An optimal weighting scheme was applied to the individual current meters to calculate the spatially averaged deep flow over a cross-stream distance equal to one

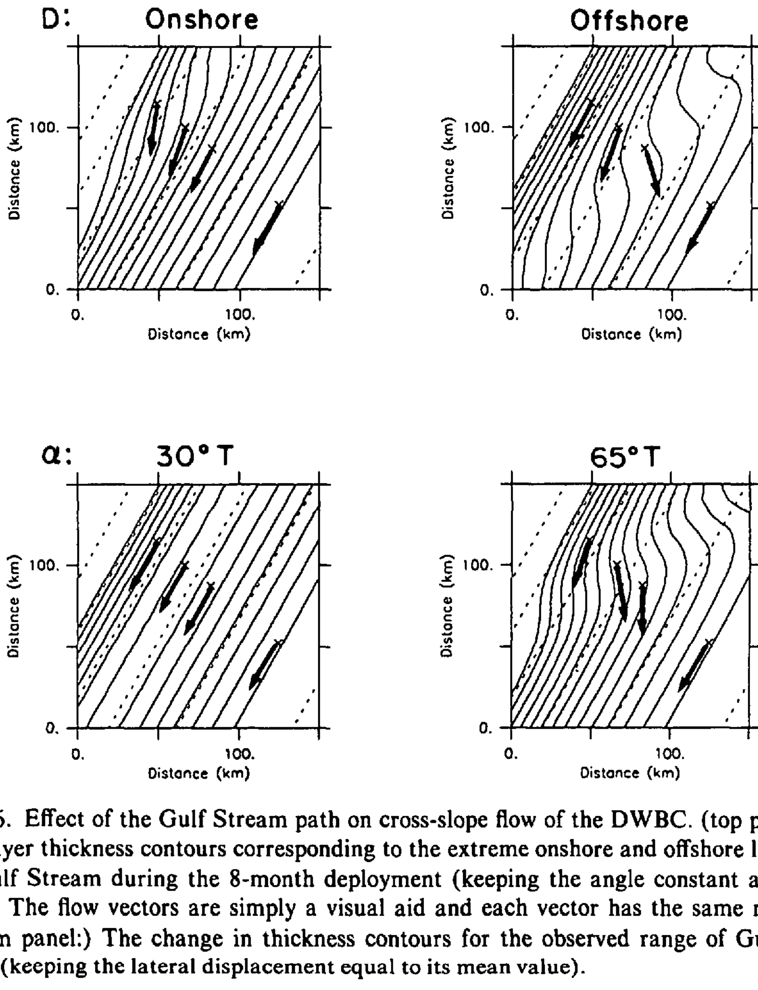

Figure 16. Effect of the Gulf Stream path on cross-slope flow of the DWBC. (top panel:) The deep layer thickness contours corresponding to the extreme onshore and offshore locations of the Gulf Stream during the 8-month deployment (keeping the angle constant at its mean value). The flow vectors are simply a visual aid and each vector has the same magnitude. (bottom panel:) The change in thickness contours for the observed range of Gulf Stream angles (keeping the lateral displacement equal to its mean value).

wavelength (130 km) of the 40 day topographic wave. In this way the wave signal is removed at each instant in time revealing the fluctuations of the DWBC itself. In contrast to the wave motions which move slightly across the topography, the weaker DWBC fluctuations are aligned more along the isobaths (with a downslope component at long periods).

Using the inverted echo sounders in conjunction with the current meters, the relationship between the upper layer Gulf Stream and deep flow was explored. Even in the presence of the strong topographic wave signal, the Gulf Stream was found to influence the deep flow at certain sites. Interestingly, the alongslope flow of the DWBC is sensitive to changes in the onshore/offshore position of the Gulf Stream, and on occasion the cross-stream averaged deep flow reverses to the northeast with the Gulf Stream. In contrast to this, fluctuations in the cross-slope flow of the DWBC are associated with changes in angle of the Gulf Stream. This observed relationship is consistent with the notion that water parcels in the DWBC want to preserve their layer thickness, which in turn implies that the DWBC should move downslope in response to its crossing the Gulf Stream. The mean vectors over the 8-month period support this dynamical interpretation as well.

Acknowledgments. The authors would like to thank Karen Tracey and Hyun-Sook Kim for their help in processing and analyzing the IES data. This work was funded by ONR contract N00014-87K-0235.

REFERENCES

Barrett, J. R. 1965. Subsurface currents off Cape Hatteras. Deep-Sea Res., *12,* 173–184.

Cronin, M. and D. R. Watts. 1989. Variability of the Gulf Stream Thermocline. Trans. Amer. Geophys. Un., *70,* 360.

Halkin, D., T. A. Rago, and T. Rossby. 1985. Data report of the Pegasus program at 73W. Technical report No. 85-2, University of Rhode Island.

Hall, M. M. 1986. Horizontal and vertical structure of the Gulf Stream velocity field at 68W. J. Phys. Oceanogr., *16,* 1814–1828.

Hogg, N. G. 1981. Topographic waves along 70W on the continental rise. J. Mar. Res., *39,* 627–649.

Hogg, N. G., and H. Stommel. 1985. On the relationship between the deep circulation and the Gulf Stream. Deep-Sea Res., *32,* 1181–1193.

Johns, W. E. and D. R. Watts. 1986. Time Scales and structure of topographic Rossby waves and meanders in the deep Gulf Stream. J. Mar. Res., *44,* 267–290.

Joyce, T. M., C. Wunsch and S. D. Pierce. 1986. Synoptic Gulf Stream velocity profiles through simultaneous inversion of hydrographic and acoustic doppler data. J. Geophys. Res., *91,* 7573–7585.

Leaman, K. D. 1989. Relationship of Gulf Stream meandering to the strength and location of the Deep Western Boundary Current. Trans. Amer. Geophy. Un., *70,* 364.

Louis, J. P. and P. C. Smith. 1982. The development of the barotropic radiation field of an eddy over a slope. J. Phys. Oceanogr., *12,* 56–73.

Luyten, J. R. 1977. Scales of motion in the Deep Gulf Stream and across the continental rise. J. Mar. Res., *35,* 49–74.

Pedlosky, J. 1979. Geophysical Fluid Dynamics. Springer-Verlag, NY, 624 pp.

Pickart, R. S. 1987. The entrainment and homogenization of tracers within the cyclonic Gulf Stream recirculation gyre. Ph.D. Thesis, Massachusetts Institute of Technology and Woods Hole Oceanographic Institution, Woods Hole, MA.

Pickart, R. S., N. G. Hogg, and W. S. Smethie. 1989. Determining the strength of the North Atlantic deep western boundary current using the Chlorofluoromethane ratio. J. Phys. Oceanogr., *19,* 940–951.

Pickart, R. S. and D. R. Watts. 1990. Using the inverted echo sounder to measure vertical profiles of Gulf Stream temperature and geostrophic velocity. J. Atmos. Oceanic Tech., *7,* 146–156.

Roemmich, D. and C. Wunsch. 1985. Two transatlantic sections: meridional circulation and heat flux in the subtropical North Atlantic Ocean. Deep-Sea Res., *32,* 619–664.

Schultz, J. R. 1987. Structure and propagation of topographic Rossby waves northeast of Cape Hatteras. M.S. Thesis, Marine Sciences Program, University of North Carolina, Chapel Hill, NC. 63 pp.

Stommel, H. 1958. The abyssal circulation. Deep-Sea Res., *5*, 80–82.

Swallow, J. C. and L. V. Worthington. 1961. An observation of a deep countercurrent in the Western North Atlantic. Deep-Sea Res., *8*, 1–19.

Swift, J. H. 1984. The circulation of the Denmark Strait and Iceland-Scotland overflow waters in the North Atlantic. Deep-Sea Res., *31*, 1339–1355.

Thompson, J. D. and W. J. Schmitz. 1989. A limited-area model of the Gulf Stream: Design, initial experiments, and model-data intercomparison. J. Phys. Oceanogr., *19*, 791–814.

Thompson, R. O. R. Y. 1977. Observations of Rossby waves near Site D. Prog. in Oceanogr., *7*, 1–28.

Thompson, R. O. R. Y. and J. R. Luyten. 1976. Evidence for bottom-trapped topographic Rossby waves from single moorings. Deep-Sea Res., *23*, 629–635.

Watts, D. R. 1989. Deep currents on the continental slope and rise in the mid-atlantic bight. Trans. Amer. Geophys. Un., *70*, 364.

Watts, D. R., and W. E. Johns. 1982. Gulf Stream meanders: observations on propagation and growth. J. Geophys. Res., *87*, 9467–9476.

Watts, D. R., K. L. Tracey and A. I. Friedlander. 1989. Producing accurate maps of the Gulf Stream thermal front using objective analysis. J. Geophys. Res., *94*, 8040–8052.

Welsh, E. B., N. G. Hogg, R. M. Hendry. 1989. The relationship of low frequency deep variability near the Hebble site to Gulf Stream fluctuations. Deep-Sea Res. (in press).

Worthington, L.V. 1976. On the North Atlantic circulation. The Johns Hopkins Oceanographic Studies, *6*, 110 pp.

—— 1970. The Norwegian Sea as a Mediterranean basin. Deep-Sea Res., *17*, 77–84.

Received: *14 February, 1990;* revised: *21 August, 1990.*